

# Complete Modeling of an Ultrasonic NDE Measurement System - An Electroacoustic Measurement Model

Changjiu Dang and Lester W. Schmerr Jr.

Center for NDE and the Department of Aerospace Engineering and  
Engineering Mechanics Iowa State University Ames, Iowa 50011  
changj@cnde.iastate.edu lschmerr@cnde.iastate.edu

## Abstract

Ultrasonic NDE measurement systems are complex systems with many electrical, electromechanical, and acoustic components. Thus, modeling has always played an important role in ultrasonics in order to characterize and understand the measurement process. It will be shown how models can simulate all the elements of the measurement process, including the pulser/receiver, cabling, transducer(s), and the acoustic/elastic waves fields, and be combined to form what is called the *electroacoustic measurement model*. It will be demonstrated how this *electroacoustic measurement model* can be used to conduct a number of parametric transducer and system studies and how the model can form the basis for experimentally characterizing all the elements of the ultrasonic measurement system, using purely electrical measurements.

## I. INTRODUCTION

A typical ultrasonic NDE immersion inspection system is shown in Fig. 1. It consists of a pulser/receiver, cabling, transducer(s), and a particular acoustic propagation/scattering configuration. For the case shown in Fig. 1 the acoustic configuration includes a fluid, an immersed component, and the flaw that is being examined.

The electrical and electromechanical components of this system (pulser/receiver, cabling, transducers) have traditionally been modeled as 1-D equivalent circuits consisting of "lumped" elements such as electrical sources, impedances, etc. The Mason and KLM transducer models, for example, are well-known models of this type<sup>(1)</sup>. However, for transducer design studies the transducer transfer matrix model of Sittig<sup>(2)</sup> is often more convenient

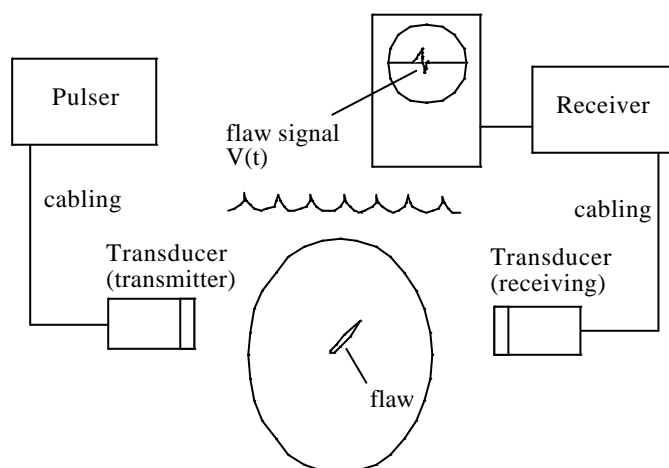


Figure 1. An ultrasonic immersion flaw inspection system

to use, as we will show later in our discussion of the influence of bonding layers on transducer response. At ultrasonic frequencies, cabling plays an important role in the measurement process and so must be modeled explicitly. A transmission line model characterized by a 2x2 transfer

matrix will be used here<sup>(3)</sup>. We should point out that in acoustic systems, which often operate at much lower frequencies, cabling effects are essentially non-existent, and are not included when performing calibration measurements, etc. Cabling effects cannot be ignored when adopting

acoustic calibration methods to ultrasonic NDE systems, as will be discussed below.

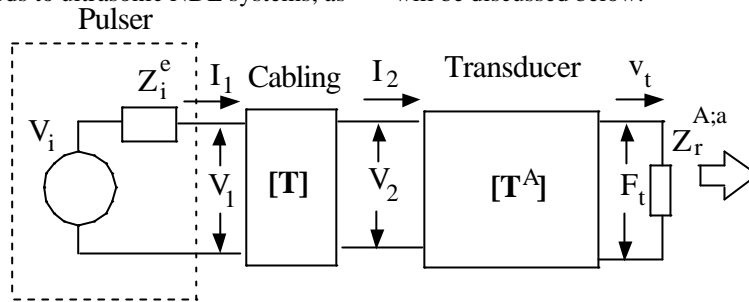


Figure 2. The ultrasound generation process components

The acoustic wave propagation and scattering fields present in an ultrasonic inspection are inherently 3-D in nature and it is not immediately obvious how to link those fields to 1-D electrical and electromechanical models of the type discussed above. The reciprocity-based relation developed by Auld<sup>(4)</sup> provides a general way to make that connection, and the measurement modeling approach of Thompson and Gray<sup>(5)</sup>, which is based on Auld's general relation, provides the means for modeling the 3-D acoustic fields as a product of 1-D models which characterize acoustic effects such as beam diffraction (on transmission and reception), material attenuation, and flaw scattering. Unfortunately, to date the 1-D electrical and electromechanical models have not been interfaced to their equivalent 1-D acoustic counterparts in a completely consistent and straightforward fashion. The recently developed *electroacoustic measurement model* that we have developed<sup>(6)</sup> does make that connection, and thus can lead to a completely 1-D model of the entire measurement

process that can be used, as we will show, for a number of important design studies.

When modeling systems with commercial electrical and electromechanical components, such as the transducers, pulser/receiver etc., it is not feasible to treat the components in terms of detailed models since many of the design features of those components are not known. Thus, it is important to be able to experimentally characterize all the system components in terms of as few parameters as possible. By using the *electroacoustic measurement model*, we will demonstrate that it is practical to formulate the system response in terms of a set of parameters that can all be obtained through purely electrical measurements in standard calibration setups. We will also show that with such a completely characterized system it is possible to combine the measured parameters and predict the directly measured system output.

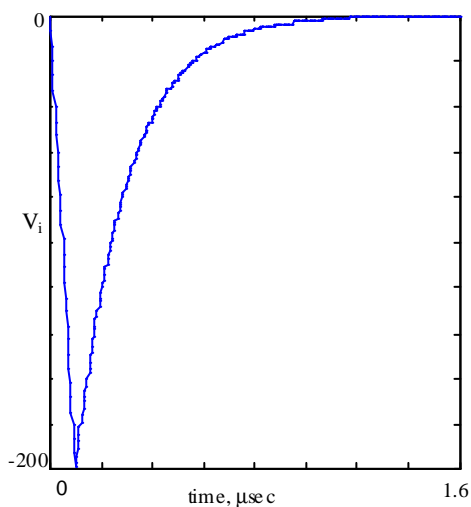


Figure 3. Model of a pulser voltage output

## II. THE GENERATION PROCESS MODEL

### Pulser

In the process of generating the acoustic fields used for inspection, the typical components involved are the pulser, the cabling connecting the pulser to an ultrasonic transducer, the transducer itself, which usually contains a piezoelectric crystal, and the fluid into which the sound is radiated, as shown in Fig. 1. In the *electroacoustic measurement (EAM) model*, the circuitry of the pulser, which is often rather complex, is replaced by a Thevenin equivalent voltage source and internal impedance whose frequency domain values (for  $\exp(-i\omega t)$  time dependency) are given by  $V_i(\omega)$  and  $Z_i^e(\omega)$ , respectively, as shown in Fig. 2. Many modeling studies in the literature omit the internal impedance and model the voltage source alone as a given time domain input. Since many commercial pulsers generate short, spike-like negative pulses, an appropriate time domain model of the pulser voltage output,  $V_i(t)$ , is

$$V_i(t) = \begin{cases} 0 & t \leq 0 \\ -V_\infty [1 - \exp(-\mathbf{a}_1 t)] & 0 \leq t \leq t_0 \\ -V_0 \exp(-\mathbf{a}_2(t - t_0)) & t \geq t_0 \end{cases} \quad (1)$$

where

$$V_\infty = \frac{V_0}{[1 - \exp(-\mathbf{a}_1 t_0)]} \quad (2)$$

so that the output voltage is given in terms of four parameters  $V_0, \mathbf{a}_1, \mathbf{a}_2, t_0$ . An analytical expression for  $V_i(\omega)$  then follows by taking the Fourier transform of  $V_i(t)$ . The explicit  $V_i(\omega)$  form will not be given here. Figure 3 shows a typical pulse generated with Eq. (1).

### Cabling

The cabling is modeled in the EAM model as a transmission line<sup>(3)</sup> whose properties can be described by a 2x2 transfer matrix, [T], where the components

$$[T] = \begin{bmatrix} \cos(k_c l_c) & -i Z_0^e \sin(k_c l_c) \\ -i \sin(k_c l_c) / Z_0^e & \cos(k_c l_c) \end{bmatrix} \quad (3)$$

relate the voltages ( $V_1, V_2$ ) and currents ( $I_1, I_2$ ) shown in Fig. 2 through the relation

$$\begin{bmatrix} V_1 \\ I_1 \end{bmatrix} = \begin{bmatrix} T_{11} & T_{12} \\ T_{21} & T_{22} \end{bmatrix} \begin{bmatrix} V_2 \\ I_2 \end{bmatrix} \quad (4)$$

where  $k_c$  is the wave number of signals propagating in the cable,  $l_c$  is the length of the cable, and  $Z_0^e = \sqrt{\mathbf{m} / \mathbf{e}}$ , and where  $\mathbf{m}$  and  $\mathbf{e}$  are the permeability and permittivity of the cable, respectively.

### Transducer

A piezoelectric ultrasonic transducer is a relatively complex component to model since it involves electrical, electromechanical, and acoustic elements. As mentioned previously, three port models such as the Mason and KLM models<sup>(7)</sup> are often used as transducer models. The three ports in these models are the electrical port, acoustic backing port at the back face of the piezoelectric crystal, and the acoustic output port at the front face of the crystal. When the type of backing is specified, both the Mason and KLM models reduce to two port models which relate the voltage and current, ( $V_2, I_2$ ) at the electrical port to the force and normal velocity, ( $F_t, v_t$ ) at the output port through a 2x2 transfer matrix,  $[T^A]$ , i.e.

$$\begin{bmatrix} V_2 \\ I_2 \end{bmatrix} = \begin{bmatrix} T_{11}^A & T_{12}^A \\ T_{21}^A & T_{22}^A \end{bmatrix} \begin{bmatrix} F_t \\ v_t \end{bmatrix} \quad (5)$$

Sittig<sup>(2)</sup> has given a model of this transfer matrix for a compressional wave transducer as a product of simple 2x2 matrices in the form  $[T^A] = [T_e^A][T_a^A]$  where

$$[T_e^A] = \begin{bmatrix} 1/n & n/i\omega C_0 \\ -i\omega C_0/n & 0 \end{bmatrix} \quad (6)$$

and

$$[T_a^A] = \frac{1}{Z_b^a - iZ_0^a \tan(kd/2)} \begin{bmatrix} Z_b^a + iZ_0^a \cot(kd) & (Z_0^a)^2 + iZ_0^a Z_b^a \cot(kd) \\ 1 & Z_b^a - 2iZ_0^a \tan(kd/2) \end{bmatrix} \quad (7)$$

The many parameters appearing in this model are as follows. The parameter  $k$  is the wave number for the piezoelectric plate, i.e.  $k = \omega / v_0$  where  $v_0$  is the wave speed of compressional waves in the piezoelectric plate given by  $v_0 = \sqrt{c_{33}^D / \mathbf{r}_P}$  in terms of the elastic constant of the plate,  $c_{33}^D$ , at constant electric flux density, and  $\mathbf{r}_P$ , the density of

the plate. The constant  $n = h_{33}C_0$  appears in the Mason model as a turns ratio of an ideal transformer. It is given in terms of  $h_{33}$ , a piezoelectric stiffness constant for the plate, and  $C_0$ , the clamped capacitance of the plate, which is given by  $C_0 = S / \mathbf{b}_{33}^S d$ , where  $S$  is the area of the piezoelectric plate,  $\mathbf{b}_{33}^S$  is the dielectric impermeability of the plate at constant strain, and  $d$  is the plate thickness. The quantity  $Z_0^a = \mathbf{r}_p v_0 S$  is the plane wave acoustic impedance of the piezoelectric plate, while  $Z_b^a(\omega)$  is the corresponding acoustic impedance of the backing (which can be a function of frequency if the backing consists of one or more layers).

The Sittig model separates out the electrical parts of the transducer ( Eq. (6)) from the acoustic parts ( Eq. (7)). It is a very convenient model to use when acoustic facing layers exist on the acoustic output port of the crystal, as they normally do for commercial transducers. A facing layer can be modeled as a 2x2 transfer matrix,  $[T_l^A]$ , that is identical in form to the transmission line cabling model where the electrical impedance of the cable,  $Z_0^e$ , is replaced by the plane wave acoustic impedance,  $Z_l^a$ , of the acoustic layer, and  $k_c$  and  $l_c$  are taken as the wave number and thickness, respectively, of the acoustic layer. Adding a

facing layer to the Sittig model is accomplished by merely incorporating the layer transfer matrix into the product of matrices already present. For a single facing layer, for example, the transducer matrix,  $[T^A]$ , is given by

$$[T^A] = [T_e^A] [T_a^A] [T_l^A] \quad (8)$$

### Radiation Impedance

The transmitting transducer  $A$  in an immersion setup radiates an acoustic wave into the surrounding fluid medium. Most 1-D transducer models account for this radiation by relating the output force and normal velocity ( $F_t, v_t$ ) through a acoustic radiation impedance, i.e.

$F_t = Z_r^{Aa} v_t$ , where the radiation impedance is taken as the specific plane wave impedance for the fluid multiplied by the area,  $S$ , of the transducer, namely

$$Z_r^{Aa} = \mathbf{r}_f c_f S \quad (9)$$

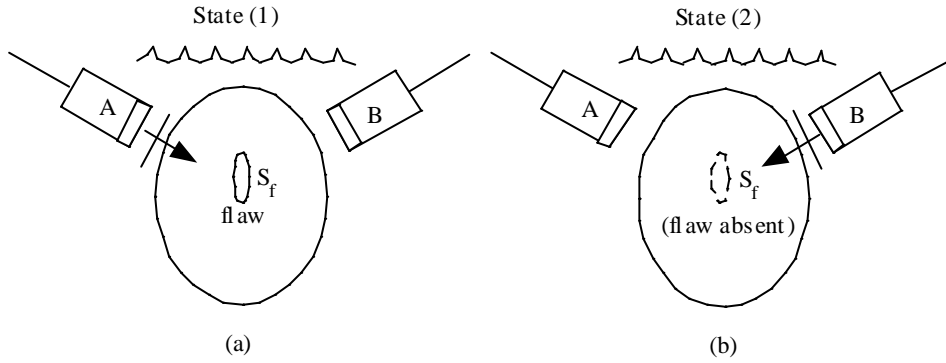


Figure 4. (a): State (1) where transducer A is firing and the flaw is present, (b): State (2) where transducer B is firing and the flaw is absent

where  $\mathbf{r}_f, c_f$  are the density and wave speed, respectively, of the fluid. However, a transducer does not generate purely plane waves and in general it is necessary to obtain the radiation impedance by solving a boundary value problem for the specific transducer being considered. Greenspan<sup>(8)</sup>, for example, has obtained the acoustic radiation impedance for a circular piston transducer of radius  $a$  in the form

$$Z_r^{Aa}(\omega) = \mathbf{r}_f c_f S \left\{ 1 - \frac{1}{k_f a} \left[ J_1(k_f a) - H_1(k_f a) \right] \right\} \quad (10)$$

where  $k_f$  is the wave number for compressional waves in the fluid and  $J_1$  and  $H_1$  are first order Bessel and Struve functions, respectively. For most ultrasonic NDE applications, the transducers used satisfy  $ka \gg 1$ , in which case Eq.(10) does reduce to the frequency independent value of Eq. (9). Note that this is not necessarily true,

though, for non-piston like transducer behavior, where using the plane wave impedance value may lead to errors.

### Generation transfer function

If one combines the cabling transfer matrix,  $[T]$ , with the transducer matrix,  $[T^A]$  to form up a "global" transfer matrix,

$$[T^G] = [T][T^A] \quad (11)$$

then it can easily be shown from Fig. 2 that the ratio of the output force,  $F_i(\mathbf{w})$ , to the Thevenin equivalent driving voltage,  $V_i(\mathbf{w})$ , is given explicitly by the generation transfer function,  $t_G(\mathbf{w})$ , where

$$t_G = \frac{F_i}{V_i} = \frac{Z_r^{A;a}}{(Z_r^{A;a}T_{11}^G + T_{12}^G) + (Z_r^{A;a}T_{21}^G + T_{22}^G)\mathcal{Z}_i^e} \quad (12)$$

This transfer function completely characterizes the entire generation process in terms of the components appearing in Fig. 2.

### III. ACOUSTIC WAVE PROPAGATION AND SCATTERING MODELS

The waves generated by the transmitting transducer travel as a beam of ultrasound into the part being inspected, scatter from any flaws present, and are received by a receiving transducer, as shown in Fig. 4a. This process is a very complex 3-D acoustic propagation and scattering problem and it appears that it difficult to combine these wave phenomena with the 1-D generation process model. However, Auld<sup>(4)</sup> has used reciprocity principles to make the connection between the acoustic fields and changes in traveling wave transmission coefficients. Auld's transmission coefficients are not directly the quantities appearing in our generation process model. But, Dang<sup>(9)</sup> has used Auld's basic approach to define the acoustic fields surrounding the flaw in terms of an acoustic transfer function,  $t_A(\mathbf{w})$ , as a ratio of a quantity called the blocked force,  $F_B(\mathbf{w})$ , at the receiver to the output force,  $F_i(\mathbf{w})$ , appearing in Eq. (12). The result is

$$t_A = \frac{F_B}{F_i} = \frac{1}{Z_r^{A;a}v_A^{(1)}v_B^{(2)}} \int_{S_f} [\mathbf{t}_{ij}^{(1)}v_i^{(2)} - \mathbf{t}_{ij}^{(2)}v_i^{(1)}] n_j dS \quad (13)$$

where  $\mathbf{t}_{ij}^{(1)}, v_i^{(1)}$  are the stresses and velocities generated in state (1) which is shown in Fig. 4a. There, the piston transducer A is firing with a normal velocity,  $v_A^{(1)}$ , on its face, and the flaw is present, where the flaw surface is  $S_f$  and the components of its outward unit normal (into the incident waves

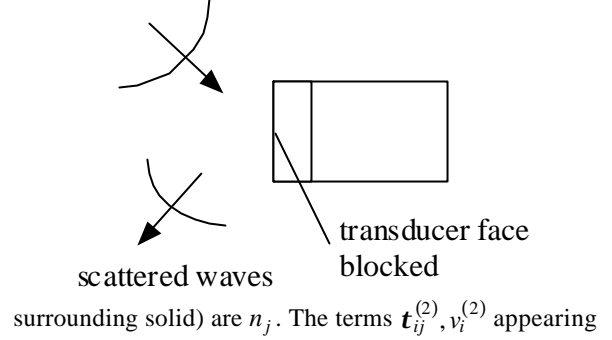


Figure 5. Incident and scattered waves on a receiving transducer when the face of the transducer is blocked.

in Eq. (13) are the stresses and velocity components, respectively, for state (2) that is shown in Fig. 4b. In state (2) the receiving transducer B (also assumed to be acting as a piston transducer) is firing with a normal velocity,  $v_B^{(2)}$ , on its face and the flaw is absent. Thus, the stresses and velocities computed on the surface  $S_f$  are just the incident waves from transducer B in state (2) while in state (1) the stresses and velocity on  $S_f$  are due to both the incident waves from transducer A and the waves scattered from the flaw.

Equation (13) gives the acoustic transfer function,  $t_A(\mathbf{w})$ , in very general terms. If we assume that the flaw is sufficiently small so that the waves incident on it are quasi-plane waves, however, this transfer function reduces to a product of explicit terms given by

$$t_A = \frac{1}{Z_r^{A;a}} V^{(1)}(\mathbf{w})V^{(2)}(\mathbf{w})A(\mathbf{w}) \left[ \frac{4\rho r_2 c_2}{-ik_2} \right] \quad (14)$$

where  $V^{(1)}, V^{(2)}$  are normalized velocities incident on the flaw for states (1) and (2), respectively (including effects of beam diffraction, material attenuation, and transmission through interfaces). The quantity  $A(\mathbf{w})$  is the plane wave far field scattering amplitude for the flaw in state (1),  $\rho$  is the density of the solid surrounding the flaw, and  $c_2, k_2$  are the wave speed and wave number for the waves incident on surface  $S_f$  in state (2). An expression similar to Eq. (14) was

first obtained by Thompson and Gray<sup>(5)</sup> in 1983 using an asymptotic analysis. Schmerr<sup>(10)</sup> later gave a less restrictive derivation of a similar result that was then used by Dang<sup>(9)</sup> to obtain Eq. (14) explicitly.

The value of Eq. (14) is that it explicitly separates out the beam propagation effects, contained in the  $V^{(1)}, V^{(2)}$  terms, from the flaw response,  $A(\mathbf{w})$ . This feature has allowed the use of deconvolution procedures to extract the

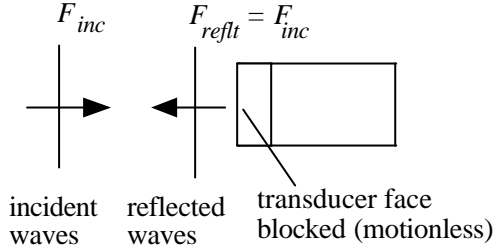


Figure 6. Modeling the incident and scattered waves as plane waves, where  $F_B = F_{inc} + F_{reflt} = 2F_{inc}$

flaw response from the total measured response and rationally perform flaw classification and sizing (see Schmerr<sup>(10)</sup>, for some examples).

The blocked force,  $F_B$ , requires some further discussion. This force is the force present on the receiving transducer when the surface of the receiver is held fixed, as shown in Fig. 5. The blocked force is the integral over the face of the transducer of the pressure,  $p^{inc}$ , due to the incident waves, and the pressure,  $p^{scatt}$ , due to the waves scattered from the blocked (motionless) receiving transducer, as shown in Fig. 5. Many authors assume that incident waves are approximately plane waves incident on the receiver and the scattered waves can be treated as purely reflected plane waves (diffraction effects neglected) at the receiver, as shown in Fig. 6. In this case, the blocked force is just twice the force,  $F^{inc}$ , in the incident waves, i.e.

$$F_B = 2F^{inc} = 2p^{inc}S_r \quad (15)$$

where  $S_r$  is the area of the receiver.

In many simple setups the acoustic transfer function,  $t_A(\mathbf{w})$ , can be obtained explicitly. One important setup that is often used for calibration purposes is shown in Fig. 7 where two transducers of the same radius,  $a$ , are aligned along their axes and separated by a distance,  $D$ , in a fluid. In this case, assuming the transducers act as pistons and that the received blocked force is just twice the force of the waves incident on the receiver, the transfer function can be expressed in the form<sup>(11)</sup>

$$t_A = 2 \exp[-\mathbf{a}(\mathbf{w})D] \left\{ \exp(ik_f D) - \frac{4p}{p_0} \int_0^{\pi/2} \sin^2 u \exp\left[ ik_f \sqrt{D^2 + 4a^2 \cos^2 u} \right] du \right\} \quad (16)$$

where  $k_f$  is the wave number and  $\mathbf{a}(\mathbf{w})$  the attenuation for the fluid.

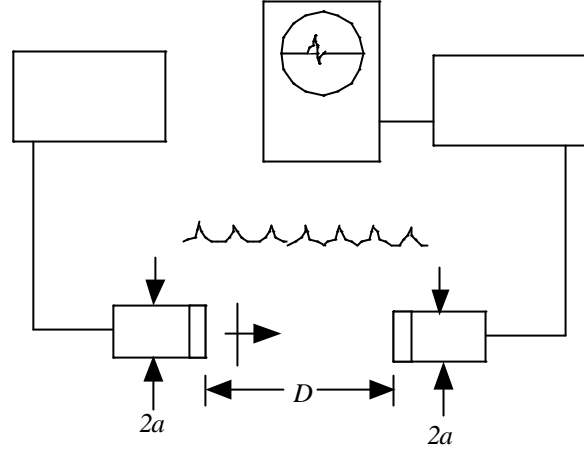


Figure 7. A reference calibration setup

#### IV. THE RECEIVING PROCESS

Figure 8 shows a model of the receiving process which is similar in form to the one we considered in Fig. 2 for the generation process. Again, the receiving transducer B and the cabling can be represented by their 2x2 transfer matrices,  $[T^B]$ , and  $[R]$ , respectively, and these transfer matrices can be combined into a single "global" 2x2 receiving matrix,  $[R^G]$ , where

$$[R^G] = [T^B][R] \quad (17)$$

It can be shown that the driving "source" for the receiving transducer in Fig. 8 is just the blocked force,  $F_B$ , at the receiver, and the impedance between this source and the transducer is equal to the acoustic radiation impedance of transducer B,  $Z_r^{B,a}(\mathbf{w})$ , when it is acting as a transmitter. Thus, if transducer B is modeled as a piston transducer and the high frequency limit is assumed, we have

$$Z_r^{B,a}(\mathbf{w}) = \mathbf{r}_{fc} S_r \quad (18)$$

with  $S_r$  the area of the receiver. In an ultrasonic NDE test, the output of the receiving transducer is normally connected

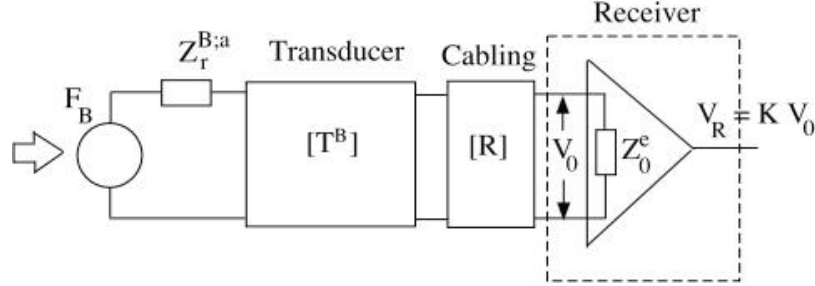


Figure 8. The ultrasound reception process components

to the receiving section of a pulser/receiver. In Fig. 7, this receiver is modeled by an equivalent electrical impedance,  $Z_0^e(\mathbf{w})$ , and a gain factor,  $K(\mathbf{w})$ .

With all the elements as shown in Fig. 8, a receiving transfer function,  $t_R(\mathbf{w})$ , can be defined as the ratio of the frequency components of the received voltage,  $V_R(\mathbf{w})$ , to the blocked force "input",  $F_B(\mathbf{w})$ , and expressed explicitly as

$$t_R = \frac{V_R}{F_B} = \frac{Z_0^e K}{(Z_r^{B;a} R_{11}^G + R_{12}^G) + (Z_r^{B;a} R_{21}^G + R_{22}^G) Z_0^e} \quad (19)$$

## V. THE ELECTROACOUSTIC MEASUREMENT MODEL

We can now combine all of our results and obtain a model of the entire ultrasonic measurement process in terms of the previously defined transfer functions as

$$\begin{aligned} V_R(\mathbf{w}) &= \frac{V_R(\mathbf{w})}{F_B(\mathbf{w})} \frac{F_B(\mathbf{w})}{F_t(\mathbf{w})} \frac{F_t(\mathbf{w})}{V_i(\mathbf{w})} V_i(\mathbf{w}) \\ &= t_R(\mathbf{w}) t_A(\mathbf{w}) t_G(\mathbf{w}) V_i(\mathbf{w}) \end{aligned} \quad (20)$$

Equation (20) represents our *electroacoustic measurement model* since it contains terms for all the electrical, electromechanical, and acoustical system elements. We should note that this EAM model is the realization of a "total system model" (see Silk et. al. <sup>(12)</sup>) more general than the one implemented in the 80's at Harwell <sup>(13)</sup>, primarily for transducer design purposes. The EAM model can also be used for transducer design, as shown in the next section,

but it also has much broader applicability in terms of system characterization and calibration.

## Transducer Design with the EAM Model

Papadakis <sup>(14)</sup> has used a model similar to the EAM model to conduct transducer parametric studies where the impedance of the backing material, the electromechanical coupling factor, and the input pulse length were varied. Another important parameter that can be examined is the thickness of the bond layer between the crystal and the front surface facing plate. To study the bond thickness we will model a transducer as a combination of the piezoelectric plate, backing, bond layer, and facing plate. Although the crystal is normally plated with a thin layer of conducting material on both its faces, in this study the effects of the plating will be ignored. The backing is often made of a mixture of epoxy and tungsten powder and is cast directly onto the plated crystal so that we do not model a bonding layer at the backing. We also model the backing itself as a semi-infinite layer so that no reflected waves are present in the backing. However, a thin bonding layer of epoxy is often present at the front face of the crystal to fix the facing to the crystal. It is the thickness of this bonding layer that will be varied in this parametric study.

In the EAM model we consider two identical transducers aligned along their axes in a fluid in a pitch-catch setup. The distance between the transducers is taken to be very small so that diffraction effects are negligible (see Eq. (16)). The material parameters were taken to be those given by Papadakis <sup>(14)</sup> as case number 69A2. The nominal

frequency of these transducers was 5 MHz and the input electrical pulse was modeled as a rectangular pulse with unit amplitude by adjusting the parameters of Eq. (1) appropriately, with the width of the pulse taken as one half the period of the fundamental free crystal response. The internal impedance of the pulser and the receiver impedance were made identical and equal to the impedance of the clamped capacitance,  $Z_c^e$ , where

$$Z_c^e = \frac{1}{2pf_0C_0} \quad (21)$$

with  $C_0$  the clamped capacitance and  $f_0$  the free crystal resonant frequency. The thickness of the epoxy bond line between the crystal and the facing plate was varied from 0.0 to 0.2 mm. In general, as the thickness increased the output voltage, which started as a single cycle waveform at zero thickness developed a higher frequency "ringing" at later times, which eventually dominated the entire response. In the frequency domain, the magnitude of the received spectrum started at zero bond thickness as a single peak at a frequency,  $F_m$ , near the nominal transducer center

frequency. At a bond thickness of about 0.05 mm a second peak in the spectrum appeared at a higher frequency,  $F_c$ , growing in size relative to the first peak until it eventually dominated the entire response at the largest bond thickness considered. These results are tabulated in Table 1 where column one lists the maximum and minimum values in the time domain waveform, column 2 lists the location of the nominal center frequency peak,  $F_m$ , and column 3 lists the location of a second, higher frequency peak,  $F_c$ , (if any). In summary, from Table 1 and other data we observe the following behavior:

a. For a very thin bonding layer the peak frequency located near the nominal center frequency dominates. A high frequency peak is not measurable.

b. As the bond thickness increases, the amplitude of the received waveforms drops rapidly. For example, as the thickness changes from 0 to 0.1 mm the peak amplitude changes from 0.05 V to 0.007 V.

Table 1. Effects of bond thickness on transducer response.

Thickness (mm)	Amplitude (V) (positive/negative)	$F_m$ (MHz)	$F_c$ (MHz)
0	0.05/-0.07	5.46	-
0.000001	0.05/-0.07	5.46	-
0.000005	0.05/-0.07	5.46	-
0.00001	0.05/-0.07	5.46	-
0.00005	0.05/-0.07	5.46	-
0.001	0.05/-0.07	5.85	-
0.005	0.05/-0.08	6.25	-
0.01	0.04/-0.06	5.46	-
0.02	0.03/-0.04	4.29	-
0.03	0.02/-0.02	3.90	-
0.04	0.01/-0.02	3.51	-
0.05	0.01/-0.01	3.12	-
0.06	0.009/-0.009	2.73	-
0.07	0.007/-0.007	2.73	-
0.08	0.007/-0.006	2.73	16.01
0.09	0.007/-0.006	2.34	14.25
0.10	0.007/-0.007	2.34	13.08
0.11	0.007/-0.007	2.34	11.91
0.12	0.007/-0.008	2.35	11.13
0.13	0.007/-0.008	2.34	10.15
0.14	0.007/-0.008	2.34	9.57
0.15	0.008/-0.009	2.34	8.78
0.16	0.009/-0.009	2.34	8.39
0.17	0.009/-0.009	2.34	7.81
0.19	0.010/-0.009	-	7.03
0.20	0.010/-0.010	-	6.64

c. As the bond thickness increases, the peak frequency also decreases but the bandwidth does not change much.

d. When the bond thickness is larger than 0.05 mm a higher frequency peak begins to appear. At larger thickness, a "bi-modal" frequency spectrum with two peaks exists for a range of thickness, but the higher frequency peak eventually dominates the measured response as the thickness continues to increase. As the higher frequency peak grows, the corresponding time-domain waveform develops a large amount of "ringing".

In conclusion, the transducer behavior is indeed very sensitive to the thickness of the bond layer between the piezoelectric crystal and the facing plate. The existence of the bonding reduces not only the waveform amplitude but also the frequency of the crystal, similar to the way the backing material "shifts down" the resonant frequency of the crystal. In the example considered a bond thickness of greater than 0.05 mm begins to have detrimental effects on the received waveform in terms of both amplitude and ringing. Thus, the bonding of the facing plate to the crystal needs to be kept very small to prevent it from affecting the output response.

## VI. COMPLETE CHARACTERIZATION OF AN ULTRASONIC SYSTEM

In design studies of the kind just discussed, one can use explicit models of each of the EAM model components to simulate the total system response. To characterize a commercial ultrasonic system, however, many of the components need to be experimentally determined since the underlying parameters are not known. For the transducers, for example, crystal material properties, backing, etc. are often not available. In the EAM model as currently described, the components that must be measured are:

Pulser: Thevenin equivalent voltage source,  $V_i(\mathbf{w})$ , and internal electrical impedance,  $Z_i^e(\mathbf{w})$

Cabling: Transfer matrix components  $(T_{11}, T_{12}, T_{21}, T_{22})$   
(for both sending and receiving cables)

Transducers: Transfer matrix components  $(T_{11}^T, T_{12}^T, T_{21}^T, T_{22}^T)$   
(for both transmitter and receiver)

Receiver: Electrical impedance,  $Z_0^e(\mathbf{w})$ , and gain,  $K(\mathbf{w})$

We will assume that the radiation impedances of the transmitting and receiving transducers are known values as given by their high frequency values for piston behavior (see Eqs. (9) and (18)) and that the acoustic transfer function can be explicitly modeled, using the Thompson-Gray approach (Eq. (14)) for a flaw measurement setup, or through an explicitly modeled calibration setup as given in Eq. (16).

The properties of the electrical components listed above can all be obtained by purely electrical calibration measurements. Characterizing the transfer matrix of a transducer, however, is another matter since it is an electromechanical device. Obtaining experimentally all four elements of the transducer transfer matrix has been called "complete transducer characterization" by Sachse<sup>(15)</sup>. To date, to our knowledge no one has developed a procedure for such a complete transducer characterization. Fortunately, all four elements of the transducer transfer matrix are not needed to model the transducer effects appearing in the generation and reception processes. In his thesis, Dang<sup>(9)</sup> has shown that it is sufficient to obtain only 1) the transducer radiation impedance (already assumed known, as mentioned above), 2) the transducer electrical input impedance, and 3) a quantity called the transducer open-circuit, blocked force receiving sensitivity. Furthermore, Dang showed that these transducer impedance and sensitivity parameters could be obtained through purely electrical measurements. The transducer electrical input impedance,  $Z_{in}^{T,e}(\mathbf{w})$ , and the open-circuit, blocked force receiving sensitivity,  $M_{V_{F_B}}^{T,\infty}(\mathbf{w})$ , were shown by Dang to be given in terms of the transducer transfer matrix,  $[T^T]$ , by

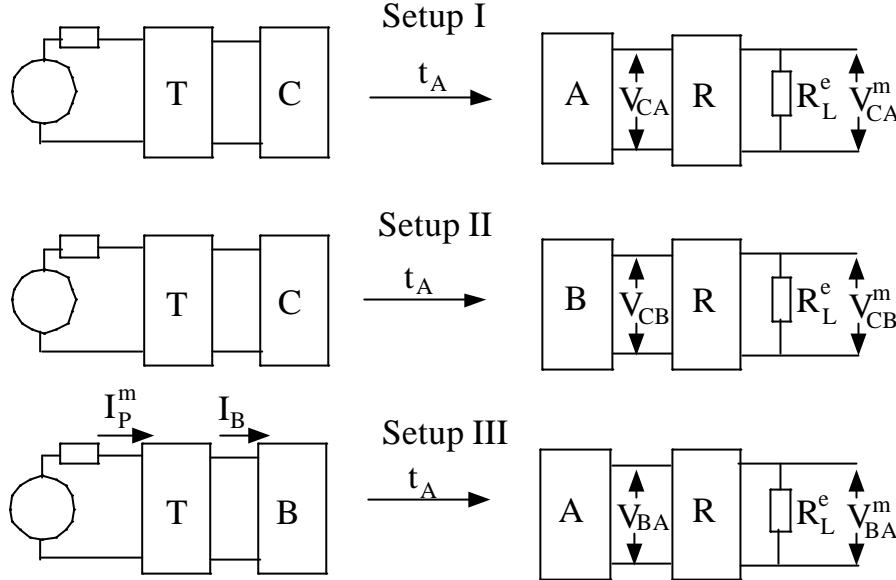
$$\begin{aligned} Z_{in}^{T,e} &= \frac{Z_r^{T;a} T_{11}^T + T_{12}^T}{Z_r^{T;a} T_{21}^T + T_{22}^T} \\ M_{V_{F_B}}^{T,\infty} &= \frac{1}{Z_r^{T;a} T_{21}^T + T_{22}^T} \end{aligned} \quad (22)$$

and that in terms of these parameters the transfer functions can be written as

$$\begin{aligned} t_G &= \frac{Z_r^{A;a} M_{V_{F_B}}^{A;\infty}}{(Z_{in}^{A,e} T_{11} + T_{12}) + (Z_{in}^{A,e} T_{21} + T_{22}) \mathcal{Z}_i^e} \\ t_R &= \frac{Z_0^e K M_{V_{F_B}}^{B;\infty}}{(Z_{in}^{B,e} R_{11} + R_{12}) + (Z_{in}^{B,e} R_{21} + R_{22}) \mathcal{Z}_0^e} \end{aligned} \quad (23)$$

where now the only transfer matrix components appearing are those for the transmitting cabling,  $[T]$ , and the receiving cabling,  $[R]$ . To make Eq. (23) useful for obtaining these

and receiving transducer (B). Dang found the input impedance simply by measuring the voltage and current inputs to the transducer when it was being used as a transmitter. For the measurement of sensitivity, Dang used a



transfer functions, one needs to be able to measure the input impedances and sensitivities of the sending transducer (A)

modification of a three-transducer reciprocity-based

Figure 9. Three transducer calibration setups for characterizing the receiving sensitivity of transducer A, using two uncalibrated transducers B and C and reciprocity principles. The measured quantities are indicated with "m" superscripts.

calibration procedure borrowed from acoustics<sup>(16)</sup>. The three-transducer setup that must be used in ultrasonics is shown in Fig. 9 where the sensitivity of transducer A is to be determined with the help of two other uncalibrated transducers B and C. Since in an immersion setup it is often impractical to measure voltages directly at the receiving transducer (which is in the fluid), voltages must instead be measured at the end of a receiving cable terminated under some known resistance loading,  $R_L^e$ . As shown in Fig. 9, three output voltage measurements ( $V_{CA}^m, V_{CB}^m, V_{BA}^m$ ) and one input current measurement ( $I_P^m$ ) are made in setups I, II, and III, where the same pulser settings, cabling, and acoustic configuration are used for all three setups. In acoustics, where the frequencies are much lower, the effects of the cables are negligible and if one takes  $R_L^e = \infty$  (open-circuit conditions), one can measure directly the open-circuit output voltages ( $V_{CA}^\infty, V_{CB}^\infty, V_{BA}^\infty$ ) and the current,  $I_B$ , at the transducers in these three setups. It can then be shown that the open-circuit, blocked force receiving sensitivity of transducer A,

which is defined as the ratio of the open-circuit output voltage of A,  $V^{A:\infty}$ , divided by the blocked force, i.e.

$$M_{V_{F_B}}^{A:\infty} = \frac{V^{A:\infty}}{F_B} \quad (24)$$

can be found from the relationship<sup>(9)</sup>

$$M_{V_{F_B}}^{A:\infty} = \sqrt{\frac{V_{CA}^\infty V_{BA}^\infty}{V_{CB}^\infty I_B} \frac{1}{Z_r^{B;a} t_A}} \quad (25)$$

However, at ultrasonic frequencies, cabling effects cannot be ignored and even if one takes open-circuit conditions at the end of the receiving cables, the voltages measured there are not the open-circuit voltages at the transducer terminals. Thus, Dang<sup>(9)</sup> defined a generalized transducer receiving sensitivity (under a general impedance loading  $Z_0^e$  at the transducer electrical port),  $M_{V_{F_B}}^A$ , given by

$$M_{V_{F_B}}^A = \sqrt{\frac{V_{CA} V_{BA}}{V_{CB} I_B \left(1 + Z_{in}^{B:e} / Z_0^e\right)} \frac{1}{Z_r^{B;a} t_A}} \quad (26)$$

Furthermore, he showed that the terms appearing in Eq. (26) could be related to the actual measured voltages and currents in Fig. 9 through the relations

$$V = \left( R_{11} + \frac{R_{12}}{R_L^e} \right) V^m \quad (27)$$

$$I_P^m = \left( Z_{in}^{B:e} T_{21} + T_{22} \right) I_B$$

where  $V$  and  $V^m$  can be any of the voltages appearing in Fig. 9 and the components of the cabling transfer matrices ( $[T]$ ,  $[R]$ ) are assumed to have been measured independently along with the electrical input impedance,  $Z_{in}^{B:e}$ . Once the generalized sensitivity of the transducer is found from Eq. (26), Dang showed that the open-circuit

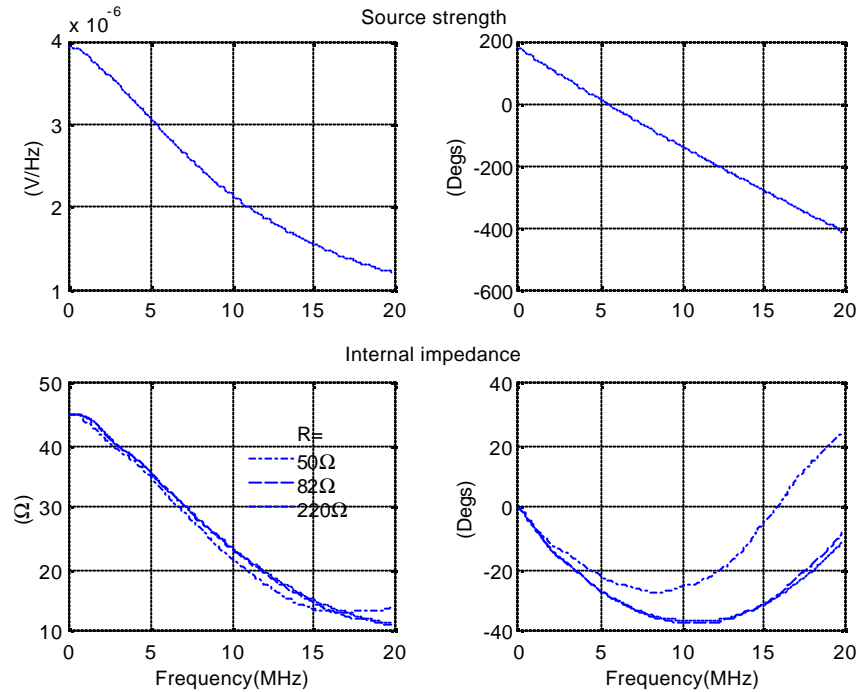


Figure 10. The Thevenin equivalent voltage source and internal impedance measured for the 5052PR pulser/receiver under external loads of 50, 82, and 220 ohms.

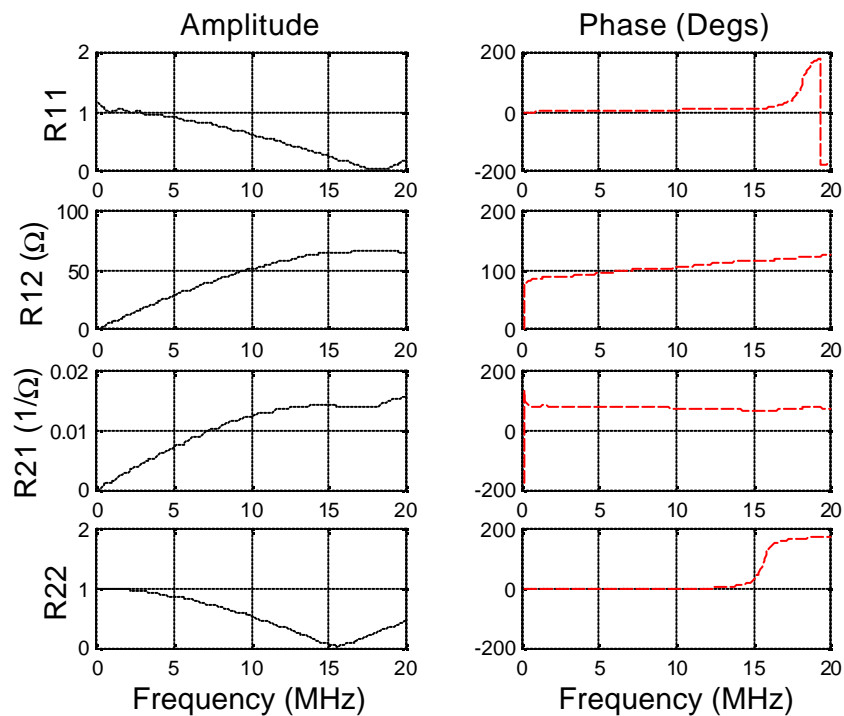


Figure 11. The transfer matrix components measured for the receiving cable

sensitivity, which is in the transfer function expressions, can be obtained from

$$M_{VF_B}^{A;\infty} = M_{VF_B}^A \left( 1 + \frac{Z_{in}^{A:e}}{Z_0^e} \right) \quad (28)$$

where the receiving load,  $Z_0^e$ , is given in terms of the receiving cabling and termination resistance as

$$Z_0^e = \frac{R_L^e R_{11} + R_{12}}{R_L^e R_{21} + R_{22}} \quad (29)$$

## VII. EXPERIMENTAL RESULTS

From the results of the previous section, it follows that the output voltage frequency components,  $V_R(\mathbf{w})$ , given by Eq. (20) as

$$V_R(\mathbf{w}) = t_R(\mathbf{w}) \mathbf{Y}_A(\mathbf{w}) t_G(\mathbf{w}) V_i(\mathbf{w}) \quad (30)$$

can be explicitly found by measuring/modeling the following terms:

**Pulser:** Thevenin equivalent voltage source,  $V_i(\mathbf{w})$ , and internal electrical impedance,  $Z_i^e(\mathbf{w})$

**Cabling:** Transfer matrix components  $(T_{11}, T_{12}, T_{21}, T_{22})$  (for both sending and receiving cables)

**Transducers:** Transducer input impedance,  $Z_{in}^{T:e}(\mathbf{w})$ , open-circuit, blocked force receiving sensitivity,  $M_{VF_B}^{T;\infty}(\mathbf{w})$ , and acoustic radiation impedance,  $Z_r^{T:a}(\mathbf{w})$  (for both transmitter and receiver)

**Receiver:** Electrical impedance,  $Z_0^e(\mathbf{w})$ , and gain,  $K(\mathbf{w})$

**Acoustic transfer function:**  $t_A(\mathbf{w})$

Many of the details of the measurement procedures required to obtain these terms will not be given here, but we will illustrate some typical results of those measurements for an acoustic configuration where two nominally identical commercial transducers are aligned along their axes in a water tank, separated by a distance  $D = 0.444\text{m}$ . A commercial pulser/receiver (Panametrics 5052 PR) was used

and 50 ohm cabling and immersion tank test fixturing existed on the transmission and receiving ends.

### Pulser

The Thevenin equivalent voltage source and impedance obtained by measuring the pulser output voltage and current at a particular energy and damping setting of the pulser/receiver are shown in Fig. 10 (both magnitude and phase shown). Theoretically, these parameters should be independent of the impedance loading at the pulser output terminals, but we did find some dependency of the internal impedance values obtained on the load.

### Cabling

By making voltage and current measurements of the cabling at different termination conditions, it is possible to determine all the transfer matrix components of the cable. Figure 11 shows those components (both magnitude and phase) for the receiving cable. Similar measurements were also carried out for the cabling on the generation side of the system. As can be seen from Fig. 11, these components do exhibit sine and cosine behavior similar to the theoretical model predictions (Eq. (3))

### Transducer sensitivity

The three-transducer reciprocity technique described previously was used to obtain the sensitivities of both the sending and receiving transducers. Figure 12 shows three sensitivity curves (for both magnitude and phase) obtained for one of the commercial transducers used in the two-transducer acoustic pitch-catch setup described previously. The dashed line in Fig. 12 shows the generalized sensitivity that would be obtained if the measured voltages and currents were used directly in the sensitivity expression (Eq. (26)) without compensating for the cabling. The solid line gives the generalized sensitivity found when cabling effects were included. Finally, the dash-dot line gives the open-circuit sensitivity calculated from the generalized sensitivity according to Eq. (28). It is this open-circuit sensitivity that goes into the generation and reception transfer functions. Fig. 12 shows that ignoring cabling effects at these ultrasonic frequencies can lead to large errors in obtaining the open-circuit sensitivity.

### Transducer input impedance

We also measured the transducer input impedance, as shown in Fig. 13, using three different methods. In the first method, we simply measured both the input voltage and

current with the transducer immersed in water. In the second method, we made a series of voltage measurements

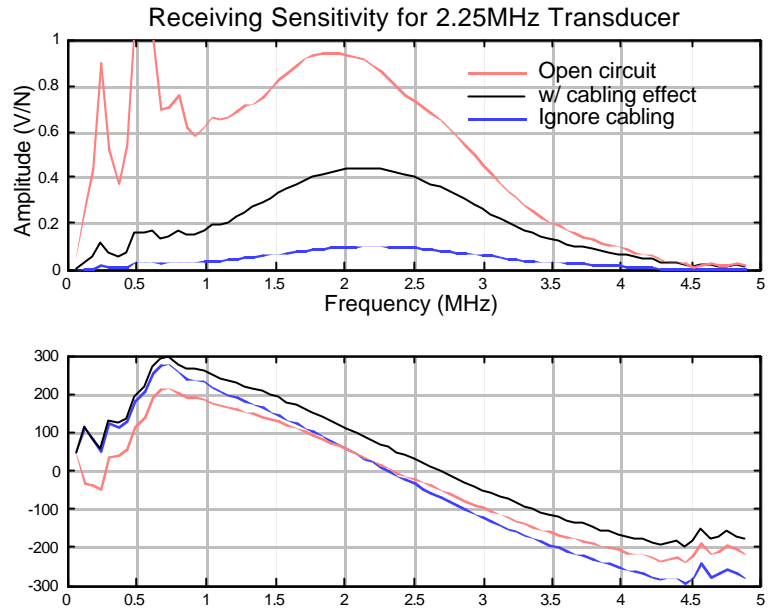


Figure 12. Transducer sensitivity measurements. Top curves – amplitude, Bottom curves – phase (deg).

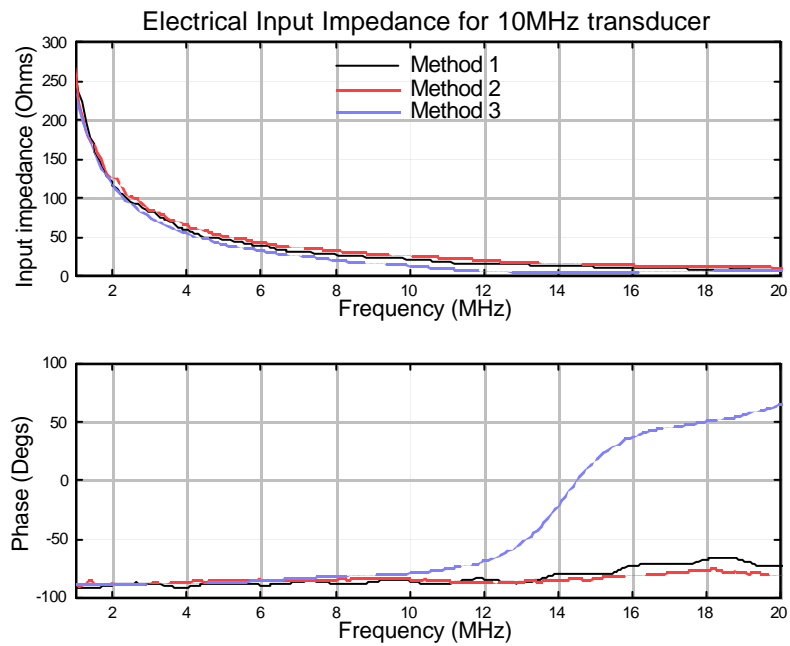


Figure 13. Transducer electrical input impedance measurements made with three different experimental

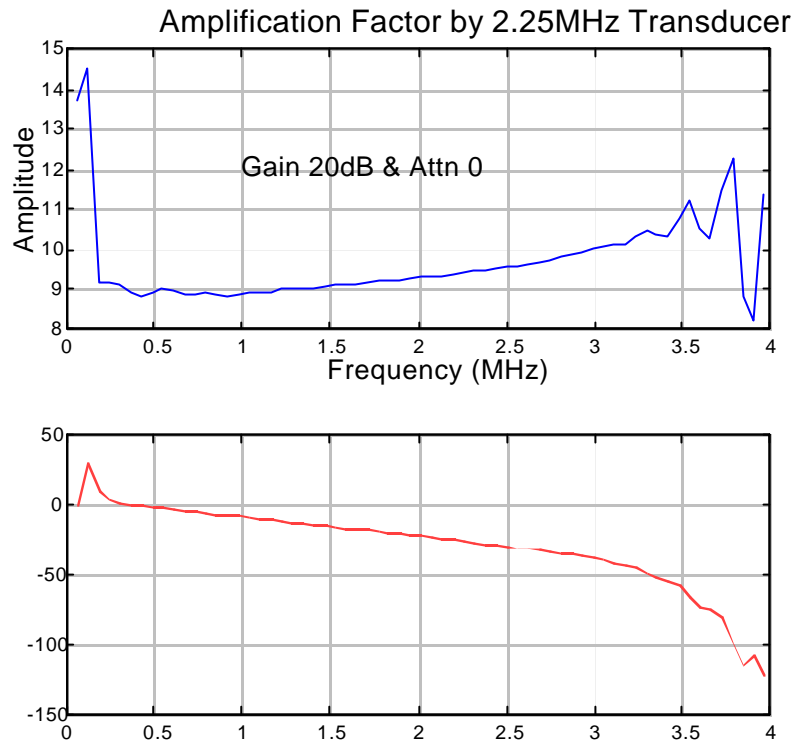


Figure 14. Measured receiver gain factor,  $K(\omega)$   
Top curve –amplitude, Bottom curve –phase (deg)

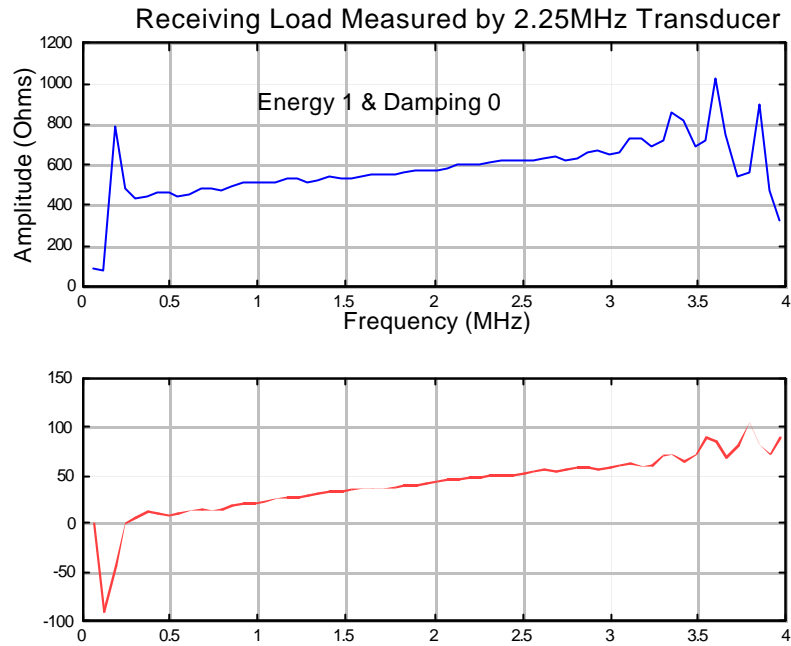


Figure 15. Measured receiver impedance,  $Z_0^e(\omega)$ .  
Top curve –amplitude, bottom curve –phase (deg)

suggested to us by the transducer manufacturer. Finally, in the third method we used an impedance analyzer. When measuring 2.5 MHz and 5 MHz transducers all three methods gave reasonably close agreement in both the magnitude and phase of the impedance versus frequency. But for 10 MHz probes the impedance analyzer showed a phase shift at higher frequencies that was not present in the results of the other two methods, as shown in Fig. 13. We believe that this phase shift was an artifact of the fixture used to connect the impedance analyzer to the transducer, and was not characteristic of the transducer itself. From Fig. 13 we can see that this transducer has an impedance curve very similar to that of a capacitor. This is not surprising since to first order a plated piezoelectric crystal does act like a capacitor. However, if electrical "tuning" circuits are also present in a transducer (which they apparently were not in this case), we cannot expect to see this capacitor-like behavior.

### Receiver gain and impedance

The receiver was set to a gain setting of 20dB, and voltage measurements made at both the receiver input and output for the measurement configuration described previously. Theoretically, such a gain setting should produce an amplification factor of 10 for all frequencies if the amplifier in the receiver was perfect. Figure 14 shows the actual gain varied from about 9 to 10 over the bandwidth of

the transducers (which in this case were 2.25 MHz transducers). Similarly, by making both voltage and current measurements at the receiver we obtained the receiver electrical impedance, as shown in Fig. 15. As can be seen from that figure, the impedance varied from about 400 to 600 ohms over the bandwidth of the transducers, with very little structure in the phase.

### Acoustic transfer function

Unlike the other transfer functions, we used an explicit model (Eq. (16)) to directly obtain the acoustic transfer function,  $t_A(\omega)$ . We took the fluid as water (wave speed = 1480 m/sec) with a frequency dependent attenuation coefficient,  $\alpha(\omega)$ , which is given in Schmerr<sup>(10)</sup>. The radius of the transducer is taken as  $a = 3.175$  mm, and the distance  $D = 444$  mm, as mentioned previously. For these parameters, the magnitude and phase of  $t_A(\omega)$  are plotted versus frequency in Fig. 16. From that figure, we see that  $t_A(\omega)$  acts like a filter with a peak response occurring in this case at a frequency of about 6.8 MHz. This behavior is expected since beam diffraction effects at low frequencies force this function to zero while the material attenuation drives the response to zero at high frequencies.

### System output simulation

Having measured or modeled all the elements that define the transfer functions appearing in the *electroacoustic measurement model*, these functions together with the Thevenin equivalent pulser voltage source can be used to obtain the frequency components of the output voltage of the entire measurement system,  $V_R(\omega)$ , as shown in Eq. (20). Taking the inverse FFT of  $V_R(\omega)$  then gives the output voltage time domain waveform which can be compared with the actual measured output waveform. In Fig. 17 we show such a comparison where the voltage was not fed through the receiver but instead was measured directly (under open-circuit conditions) at the end of the receiving cable for the calibration setup of Fig. 7. From Fig. 17 we see that there is very good agreement with the EAM model predictions and the measured results. To our knowledge, this is the first demonstration of completely characterizing all the components of an ultrasonic system and then assembling those components in an explicit fashion (through the EAM model) to predict the total system response.

## VIII. CONCLUSIONS AND DISCUSSION

We have described the *electroacoustic measurement model* and have illustrated its use in

transducer design and system characterization applications. The title of the paper indicates that the EAM model gives us a complete model of an ultrasonic NDE measurement system. To a large extent that is true, as seen from the examples we have discussed. There are, however, a number of phenomena that the EAM model does not currently address. For example, the EAM model is a noise-free model since it does not explicitly consider sources of either electronic noise or material noise. Oakley<sup>(17)</sup> has discussed a method for adding thermal and amplifier noise to the system, and Margetan et. al.<sup>(18)</sup> describe a methodology for predicting grain noise distributions that could be combined with the EAM model. Also, the EAM model as currently implemented treats all the electrical and electromechanical components as ideal (lossless) elements. However, it is not difficult to add small loss terms to the various 1-D component models

The EAM model provides a powerful tool for analyzing virtually any element in the measurement process. The examples discussed here only provide a very limited demonstration of the capabilities of the EAM model. Future applications planned include a variety of system characterization and calibration studies that will help to make ultrasonic NDE measurements more quantitative and reproducible..

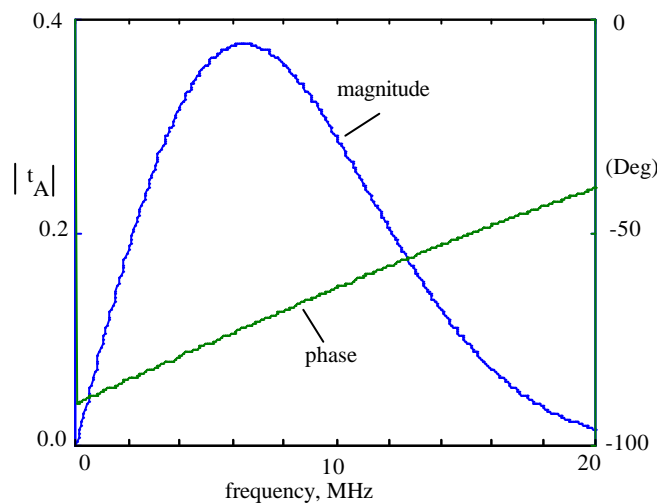


Figure16. The magnitude and phase of the acoustic transfer function

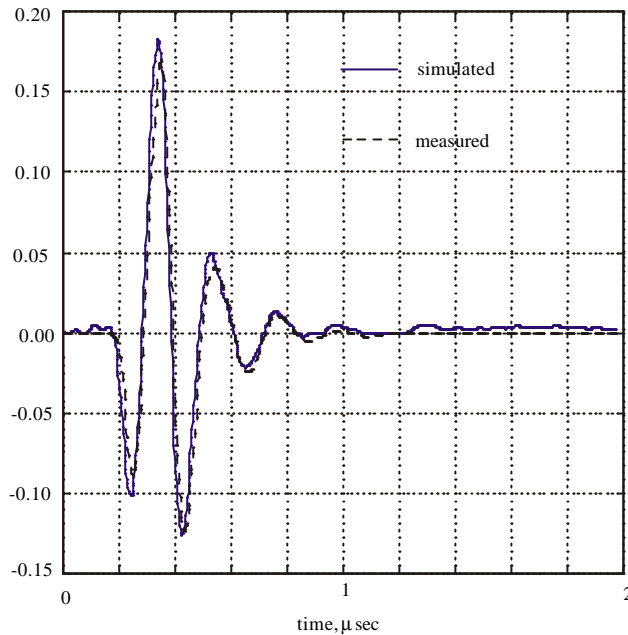


Figure 17. Simulated (solid line) and measured (dotted line) output voltage. Energy Level 1, Damping 5 settings on the pulser. Open-circuit receiving conditions.

Thompson and D.E. Chimenti, Eds., Plenum Press, New York, **18A**, 1115-1122 (1999).

## IX. ACKNOWLEDGMENT

This work was supported by the National Science Foundation Industry/University Cooperative Research Center Program at the Center for NDE, Iowa State University.

## X. REFERENCES

- 1 - Kino, G.S., "Acoustic Waves - Devices, Imaging, & Analog Signal Processing," Prentice Hall, Englewood Cliffs, New Jersey (1987).
- 2 - Sittig, E.K. IEEE Trans. Sonics and Ultrasonics, **SU-16**, 2-10 (1969).
- 3 - Pozar, D.M., "Microwave Engineering, 2nd Ed.," John Wiley, New York (1998).
- 4 - Auld, B.A. Wave Motion, **1**, 3-10 (1979).
- 5 - Thompson, R.B., and T. Gray J. Acoust. Soc. Am., **74**, 1279-1290 (1983).
- 6 - Dang, C.J, and L.W. Schmerr, in " Review of Progress in Quantitative Nondestructive Evaluation," D.O. Thompson and D.E. Chimenti, Eds., Plenum Press, New York, **18A**, 1115-1122 (1999).
- 7 - Ristic, V.M. " Principles of Acoustic Devices," John Wiley, New York (1983).
- 8 - Greenspan, M. J. Acoust. Soc. Am., **65**, 608-621 (1979).
- 9 - Dang, C.J, "An Electroacoustic Measurement Model", Ph.D. Thesis, Iowa State University, 2000 (to appear).
- 10 - Schmerr, L.W., " Fundamentals of Ultrasonic Nondestructive Evaluation - A Modeling Approach," Plenum Press, New York (1998).
- 11 - Williams, A.O., J. Acoust. Soc. Am., **23**, 1-6 (1951).
- 12 - Silk, M.G., Bainton, K.F., and M.J. Hillier, in " Mathematical Modeling in Non-destructive Testing," M. Blakemore and G.A. Georgiou, Eds., Oxford University Press, New York, 175-189 (1988).
- 13 - Silk, M.G. " Ultrasonic Transducers for Nondestructive Testing," Adam Hilger Ltd., Bristol, England, (1984).
- 14 - Papadakis, E.P., Mat. Eval., **41**, 1378-1388 (1983).

15 - Sachse, W. and N.N. Hsu, in "Physical Acoustics, Vol XIV," E.P. Mason and R.N. Thurston, Eds., Academic Press, New York, 277-407 (1979).

16 - Bobber, R.J. "Underwater Electroacoustic Measurements," Nav. Res. Lab, Washington, D.C., (1970).

17 - Oakley, C.G., IEEE Trans. Ultrasonics, Ferroelectrics, and Frequency Control, **44**, 1018-1026 (1997).

18 - Margetan, F.J., Yalda, I., and R.B. Thompson, in "Review of Progress in Quantitative Nondestructive Evaluation," D. O. Thompson and D.E. Chimenti, Eds., Plenum Press, New York, **15B**, 1509-1516 (1996).